JOURNAL OF MATERIALS SCIENCE: MATERIALS IN ELECTRONICS 2 (1991) 116–123

Reaction kinetics and optical properties of semiconducting $MnSi_{1.73}$ grown on ⟨001⟩ oriented silicon

LIN ZHANG, D. G. IVEY
Department of Mining, Metallurgical and Petroleum Engineering, University of Alberta, Edmonton, Alberta, T6G 2G6 Canada

The growth kinetics and optical properties of thin layers of $MnSi_{1.73}$ have been studied. $MnSi_{1.73}$ was formed by thermal reaction (485–570 °C) of Mn–Si thin-film couples, through a nucleation-controlled process. $MnSi_{1.73}$ is semiconducting and the band-gap energy was optically determined using a spectrophotometer and a sample with a single $MnSi_{1.73}$ layer on a silicon substrate. The value was between 0.78 and 0.83 eV.

1. Introduction

Recently, several papers [1–4] concerning semiconducting silicides have been published. Many of these semiconducting silicides are reported to be direct band-gap semiconductors, making them attractive for optoelectronic applications as well as being compatible with existing Si integrated circuit technology. One particular silicide, $MnSi_{1.73}$, discovered to be semiconducting in the mid-1970s, is believed to have a band gap energy in the infrared range, making it potentially suitable for fibre-optic applications. There is, however, some uncertainty regarding the exact value of the band gap. Nishida [5], Kawasuni *et al.* [6] and Samsonov [7] calculated band gap values for bulk samples from electrical resistivity measurements, obtaining values of 0.4, 0.703 and 0.9 eV, respectively. Krontiras *et al.* [8] have also evaluated band gap values of 0.45 and 0.42 eV from both resistivity and Hall effect data. Other recent band gap measurements were made in 1987, by Bost and Mahan [9], using samples with polycrystalline $MnSi_{1.73}$ films on Si substrates. A band gap value of 0.68 eV was determined optically.

In this paper we examine the formation of $MnSi_{1.73}$ from Mn layers deposited on Si substrates. Band gap measurements are also done on $MnSi_{1.73}$ using an optical technique, and these are compared with values in the literature.

2. Experimental

2.1. Manganese deposition and silicide formation

High-purity manganese (99.98%) was deposited by thermal evaporation onto ⟨001⟩ oriented, single-crystal silicon wafers. Prior to deposition, the silicon wafers were cleaned using buffered hydrofluoric acid (20 parts water to 1 part HF), rinsed with deionized water and dried with high-purity Ar. After an Si wafer was loaded into the deposition chamber, the chamber was pumped down to a pressure of 2×10^{-6} torr. The thickness of the Mn film, measured using cross-sectional transmission electron microscopy (TEM) of as-deposited specimens, was nominally 300 nm.

After Mn deposition, the Si wafers were cleaved into 1 cm × 1 cm pieces and loaded individually into a quartz tube furnace. Annealing was done in flowing nitrogen (purified nitrogen, 99.97%) at temperatures ranging from 485 to 570 °C for times up to 256 min. 485 °C represents the lowest annealing temperature for which $MnSi_{1.73}$ formation was detected. The results of lower-temperature anneals have been reported in a previous papers [10].

2.2. Phase identification

Phase identification and silicide growth were monitored through X-ray diffraction (XRD) and TEM techniques. A Rigaku Geigerflex X-ray diffractometer, with a scintillation counter probe and a graphite single-crystal monochromator, was used in X-ray diffraction experiments. A Co target X-ray tube operating at 50 kV and 20 mA was utilized.

Both plan-view and cross-section specimens were prepared, using standard techniques of dimpling and ion milling [11, 12], for electron microscopy investigations. Several electron microscopes were utilized, i.e. a Hitachi H-7000 TEM, a Philips 400 EM and a Hitachi H-600 TEM/STEM equipped with a Be window X-ray detector.

The techniques utilized for phase characterization included bright-field imaging, selected-area diffraction (SAD), convergent-beam electron diffraction (CBED) and energy-dispersive X-ray spectroscopy (EDX).

Phase compositions were calculated, from EDX spectra, from empirically determined k or Cliff–Lorimer factors, according to the following expression:

$$\frac{C_{Si}}{C_{Mn}} = k_{Si/Mn}\frac{I_{Si}}{I_{Mn}} \quad (1)$$

0022–2461/91 $03.00 + .12

C_{Si} and C_{Mn} are the concentrations of Si and Mn, respectively, and I_{Si} and I_{Mn} are the background-subtracted K_α X-ray intensities for Si and Mn obtained from EDX spectra. The k factor, which is independent of specimen composition, was determined from a known specimen of MnSi. A value of 1.13 ± 0.01 was obtained.

2.3. Band gap measurements

The configuration for measuring the reflection (R) and transmission (T) spectra is shown in Fig. 1a. This is an $MnSi_{1.73}$ film of complex refractive index (n-ik) on an Si substrate of complex refractive index (n_s-ik_s), surrounded by air of refractive index $n_0 = 1$. Reflection and transmission spectra were measured from this configuration using a Cary 2300 UV-Visible-NIR spectrophotometer. The optical constants for $MnSi_{1.73}$, i.e. refractive index, n, and extinction coefficient, k, were calculated from these spectra. The absorption coefficient was obtained from the following equation:

$$\alpha = 4\pi k/\lambda \tag{2}$$

where α is the absorption coefficient and λ is the wavelength of incident light used in the measurement. The band gap was then determined by plotting α^2 versus E (the photon energy corresponding to λ) and extrapolating the linear section of the plot to the intercept with the E axis. The value of the interception point, E_g, is the band gap energy.

For the configuration used in this experiment, however, the effect of multiple internal reflections on the reflection and transmission spectra had to be taken into account. Fig. 1b illustrates this complicated process. The internal multiple reflections make the exact expressions for transmitted and reflected light intensity from this configuration cumbersome and difficult to solve. In order to evaluate the optical constants, a model and an iterative procedure, developed by Brett [13], were adopted in this investigation. This model is suitable for a structure with an absorbing film on a transparent substrate. Although Si is transparent in the range of wavelength used, the absorption of the Si substrate has to be taken into account due to the relatively large thickness of the substrate. Therefore, a modification was introduced to Brett's iterative procedure (see Appendix A). After this modification, the equations used in this procedure have the following forms:

$$T = \exp\left(-\frac{4\pi kd}{\lambda}\right)\exp\left(-\frac{4\pi k_s d_s}{\lambda}\right) \times (1 - r_o)(1 - r)(1 - r_s) \tag{3}$$

$$R = r_o + \exp\left(-\frac{8\pi kd}{\lambda}\right)\left[(1 - r_o)^2 r + \exp\left(-\frac{8\pi k_s d_s}{\lambda}\right)(1 - r_o)^2(1 - r)^2 r_s\right] \tag{4}$$

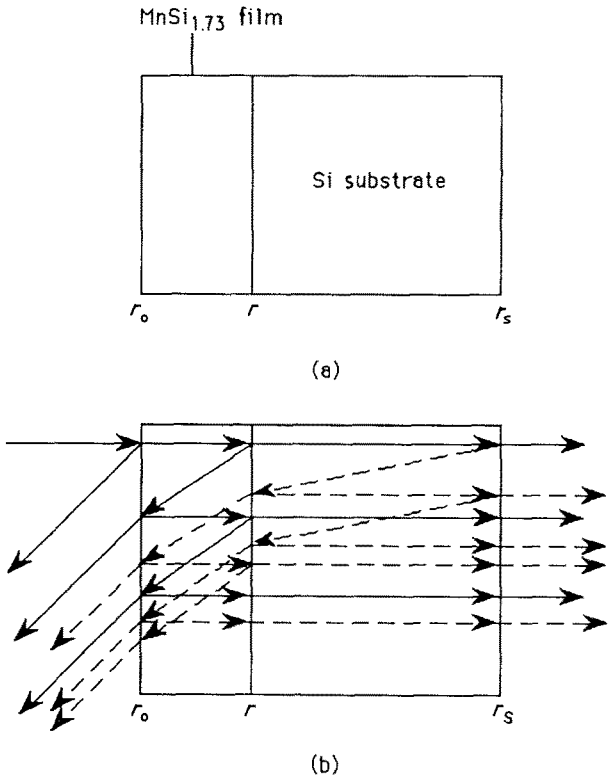

Figure 1 (a) Schematic diagram of configuration used in optical property measurements (not to scale). r_o, r and r_s are the reflectivities of interfaces air–$MnSi_{1.73}$, $MnSi_{1.73}$–Si and Si–air, respectively. (b) Schematic diagram showing multiple internal reflections; only the first two orders of reflections are shown. Solid rays represent the reflections involving multiple reflections in $MnSi_{1.73}$ film only. Dashed rays represents the reflections involving multiple reflections in both $MnSi_{1.73}$ and Si.

$$r_o = \frac{(n - 1)^2 + k^2}{(n + 1)^2 + k^2} \tag{5}$$

$$r = \frac{(n - n_s)^2 + (k - k_s)^2}{(n + n_s)^2 + (k + k_s)^2} \tag{6}$$

T and R are the measured transmission and reflection, respectively; n and k are the refractive index and extinction coefficient of the $MnSi_{1.73}$ film; n_s and k_s are the refractive index and extinction coefficient of the Si substrate; λ is the wavelength of the incident light; r_o, r and r_s are the reflectivities at each interface indicated in Fig. 1a. The variables T, R, λ, d and d_s can be experimentally determined. n_s and k_s must be evaluated using measurements from a bare Si wafer and the following equations (Appendix B):

$$r_s = \frac{-(R_s^2 - 2R_s - 1 - T_s^2) + [(R_s^2 - 2R_s - 1 - T_s^2)^2 - 4(2 - R_s)R_s]^{1/2}}{2(2 - R_s)} \tag{7}$$

$$n_s = \frac{1 + r_s^{1/2}}{1 - r_s^{1/2}} \tag{8}$$

$$k_s = -\frac{1}{2}\log\left(\frac{R_s - r_s}{R_s r_s^2 + r_s - r_s^2}\right)\left(\frac{\lambda}{4\pi d_s}\right) \tag{9}$$

R_s and T_s are the reflection and transmission measured from a bare Si sample, which was cut from the same wafer as that for a sample with an $MnSi_{1.73}$ film. After n_s and k_s were determined, n and k for $MnSi_{1.73}$ were determined by the following iterative procedure

[13]:

(i) measure R, T and d;
(ii) λ is known; calculate r_s using Equation 7;
(iii) initialize $r_o = R$ and $r = 0$;
(iv) evaluate k using Equation 3;
(v) evaluate r_o using Equation 4;
(vi) evaluate n from r_o and k using Equation 5;
(vii) calculate r from the new n and k values using Equation 6;
(viii) repeat steps (iv) to (vii).

Convergence to four-figure agreement of successive n and k values was obtained for all the experimental data of $R(\lambda)$, $T(\lambda)$ and λ.

3. Results and discussion

3.1. Formation of $MnSi_{1.73}$

The lowest temperature for which $MnSi_{1.73}$ formation was detected was 485 °C, after a minimum annealing period of 1 h. This is evident from the XRD data in Table I.

$MnSi_{1.73}$ has a complicated crystal structure. So far, it has been reported as Mn_4Si_7 [14], $Mn_{11}Si_{19}$ [15], $Mn_{15}Si_{26}$ [16] and $Mn_{27}Si_{47}$ [17]. According to Ye and Amelinckx [18], this is because the material is a one-dimensional doubly periodic crystal, i.e. a crystal in which the sublattices of the two constituents have different periods along one common direction while the other two lattice parameters are equal. The manganese atoms form a β-tin type of arrangement with a tetragonal subcell ($a = 0.552$ nm, $c_{Mn} = 0.437$ nm) (Fig. 2a). The silicon atoms adopt a double-helical arrangement (Fig. 2b), with a period equal to the pitch of this helix $c_{Si} \cong 4c_{Mn}$, filling the interstices left in the Mn sublattice. The resulting, approximately rationalized, c-period is the smallest common multiple of c_{Mn} and c_{Si}. At the present time, what causes the changes in c_{Mn} or c_{Si} is still unknown.

A representative CBED pattern for $MnSi_{1.73}$ is shown in Fig. 3. The zero-order Laue zone (ZOLZ) pattern matches with several structure variants of

TABLE I X-Ray diffracted intensities from $\{200\}_{MnSi}$ and $\{1\,1\,30\}_{MnSi_{1.73}}$ reflections

Annealing temperature (°C)	Annealing time (min)	XRD intensities from $\{200\}_{MnSi}$	XRD intensities from $\{1\,1\,30\}_{MnSi_{1.73}}$
485 ± 5	10	276	–
	30	276	–
	60	233.4	83.7
	90	201.6	98.2
	150	131.9	149.9
	196	74.5	237.5
	256	39.5	271.5
540 ± 5	10	241.5	42.6
	20	186	119.3
	30	118	182
	60	–	234.6
570 ± 5	5	294.5	51.6
	8	164.7	173.6
	16	75	244

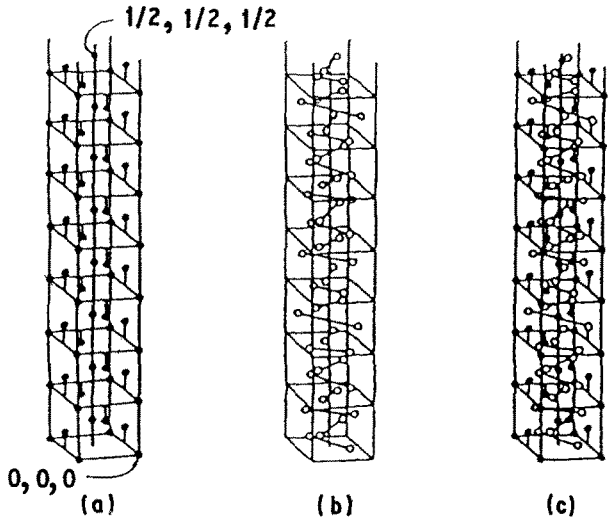

Figure 2 Sketch of the Mn and Si atoms within one-half of a unit cell of $Mn_{15}Si_{26}$ showing stacking of (a) Mn subcells, (b) Si atom pairs about the central axis, (c) Mn and Si atoms. (●) Mn, (○) Si [16].

$MnSi_{1.73}$. However, the reciprocal lattice spacing (H) for the higher-order Laue zone (HOLZ) matches best with Mn_4Si_7. H_c (calculated) is 0.3558 nm^{-1}, while H_m (measured) is 0.6813 nm^{-1}, so that $H_m = 2H_c$. The lattice parameters for Mn_4Si_7 are $a = 0.5525$ nm and $c = 1.7465$ nm. The a lattice parameter for Mn_4Si_7 is very close to the value for Si ($a = 0.5431$ nm), the relative difference only being 2.2%. Epitaxial growth of $MnSi_{1.73}$ on Si is possible as long as the $\langle 0\,0\,1 \rangle$ directions of the two materials are parallel.

Prior to $MnSi_{1.73}$ formation three silicides were observed, i.e. Mn_3Si, MnSi and Mn_5Si_3. The kinetic behaviour for these silicides is diffusion-controlled and has been discussed in detail elsewhere [10]. $MnSi_{1.73}$, on the other hand, nucleates and grows in islands instead of a layered growth manner, and only begins to form after MnSi growth has finished (Table I). Fig. 4 shows evidence of this different growth behaviour. This micrograph is from a plan-view specimen annealed at 485 °C for 60 min. In this specimen, many islands with large grains are surrounded by larger areas with small grains. From SAD, CBED and EDX analysis, it was determined that the small grains are MnSi and the large grains are $MnSi_{1.73}$.

The growth process of $MnSi_{1.73}$ is illustrated schematically in Fig. 5. $MnSi_{1.73}$ nucleates preferentially at various positions along the MnSi–Si interface, and then grows in three dimensions. As discussed below, this type of growth process is nucleation-controlled.

Nucleation-controlled processes for silicide formation have been reviewed by d'Heurle and Gas [19]. They use classical nucleation theory to discuss the phenomena encountered in thin-film reactions. According to the classical theory of nucleation, the activation energy ΔG^* for a new phase, AB, forming at an interface between two phases A and B, is proportional to $(\Delta\sigma)^3/(\Delta G)^2$. $\Delta\sigma$ indicates the increase in surface energy, because two interfaces A–AB and AB–B replace the original A–B interface during AB

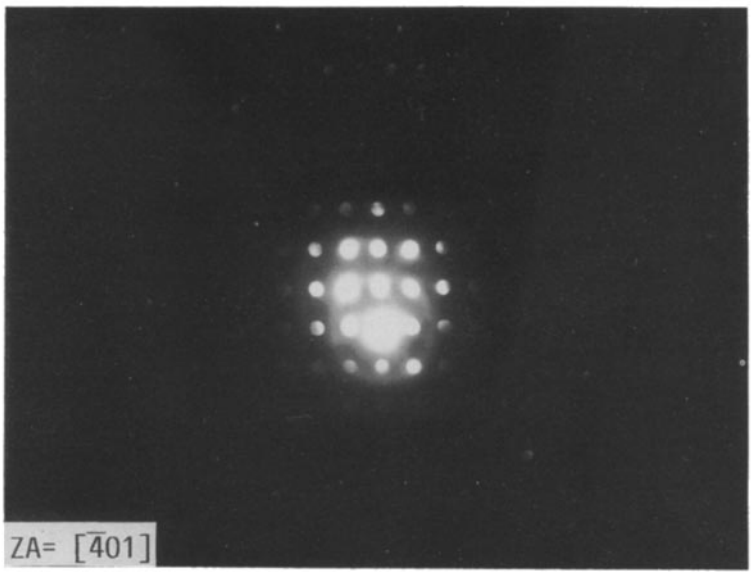

Figure 3 Indexed CBED pattern from $MnSi_{1.73}$ (zone axis = [401]).

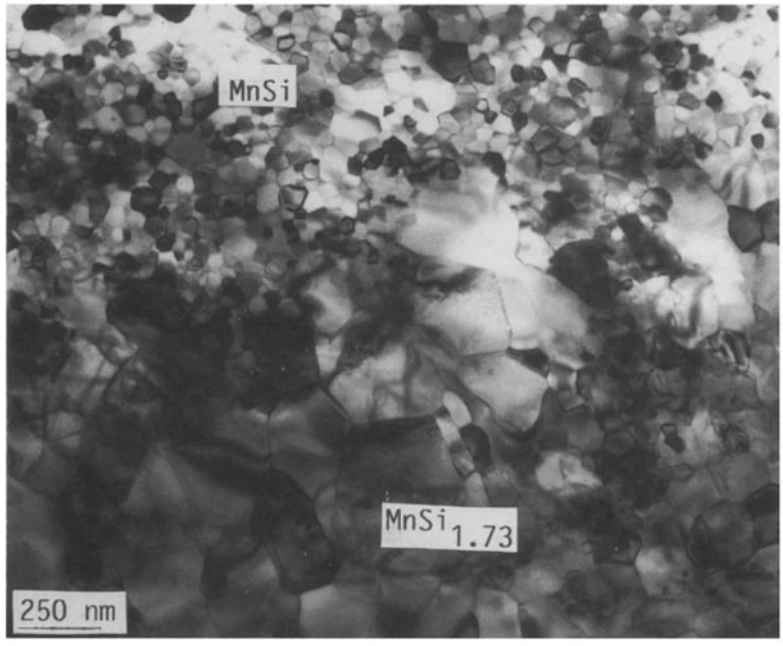

Figure 4 TEM micrograph showing island growth of $MnSi_{1.73}$.

formation; ΔG is the change of free energy per unit volume of AB and is given by

$$\Delta G = |\Delta G_c| - \Delta H_d \quad (10)$$

ΔG_c is the change in "chemical" free energy per unit volume of AB due to the formation of the new phase and ΔH_d is the deformation energy loss due to the volume change caused by phase transformation. Therefore, ΔG^* can be written as

$$\Delta G^* \propto \frac{(\Delta\sigma)^3}{(|\Delta G_c| - \Delta H_d)^2} \quad (11)$$

According to d'Heurle and Gas [19], in general, when metals and silicon react with one another to form silicides, the absolute values of ΔG are large and those of ΔG^* are small. As a result, nucleation is so easy and rapid that one cannot isolate it and observe it experimentally. However, a nucleation-controlled process will occur if the activation energy, ΔG^*, for the new silicide phase to nucleate is large and the reaction temperature is relatively low. This is the case encountered during the annealing reaction of $MnSi_{1.73}$.

From the XRD data in Table I, it is obvious that before $MnSi_{1.73}$ formation, the growth of MnSi has finished. Therefore, the formation process for $MnSi_{1.73}$ is (see Fig. 5)

$$MnSi + 0.73Si \rightarrow MnSi_{1.73} \quad (12a)$$

and not

$$Mn + 1.73Si \rightarrow MnSi_{1.73} \quad (12b)$$

The standard Gibbs free energy at 485 °C for Reaction 12a can be calculated. If data from Samsonov and Vinitskii [20] are used, the resulting value is $+24.1\ kJ\ mol^{-1}$; and if data from Chart [21] are used, the calculated value is $-12.2\ kJ\ mol^{-1}$. There exists some discrepancy between the two calculated values, which arises from the discrepancy in reported ΔH°_{298} and ΔS°_{298} values for MnSi. In either case the absolute value of ΔG° is rather small, and since the reaction actually does occur, it follows that

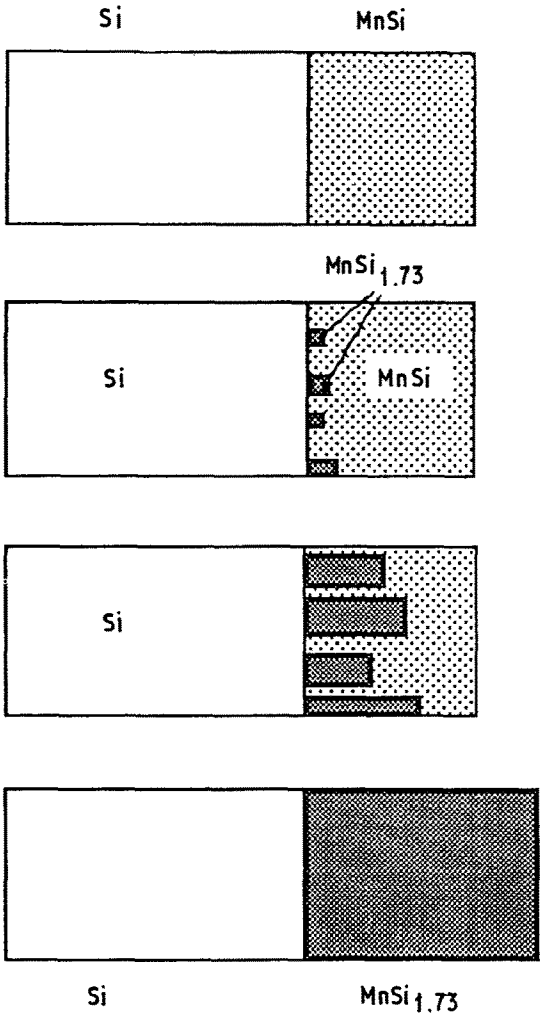

Figure 5 Schematic process of $MnSi_{1.73}$ nucleation and growth from the interface between Si and MnSi. $MnSi_{1.73}$ nucleates at some position on the interface and then these nuclei grow in three dimensions.

the standard free energy for this reaction has a small negative value.

In addition, by evaluating the ratio of the molar volumes for MnSi and $MnSi_{1.73}$, one can find that if Reaction 12a takes place, the volume increase will be about 40%:

$$\frac{\text{Molar volume of } MnSi_{1.73}}{\text{Molar volume of MnSi}} = \frac{N_{MnSi}\, n_{1Mn}}{N_{MnSi_{1.73}}\, n_{2Mn}} = \frac{4.226 \times 10^{22} \times 1}{7.53 \times 10^{21} \times 4} \cong 1.4 \quad (13)$$

N_{MnSi} and $N_{MnSi_{1.73}}$ are the numbers of formula units of MnSi and $MnSi_{1.73}$ in a unit volume (f.u. cm^{-3}), respectively; n_{1Mn} and n_{2Mn} are the atom numbers of Mn in one formula unit of MnSi and $MnSi_{1.73}$ (Mn_4Si_7), respectively. As a result of the large change in volume, the value of ΔH_d (energy change due to deformation) will be relatively high. Since

$$\Delta G^* \propto \frac{\Delta\sigma^3}{(|\Delta G_c| - \Delta H_d)^2} \quad (14)$$

the activation energy for Reaction 12a will be rather high indeed. Thus, the theory of nucleation-controlled processes can explain the island growth observed in this experiment. Nucleation-controlled kinetics was also proposed by Eizenberg and Tu [22] for the formation of $MnSi_{1.73}$, and elsewhere for the following silicides: $NiSi_2$ [19], $ZrSi_2$ [19], Rh_4Si_5 [23], Rh_3Si_4 [23], PdSi [19], $HfSi_2$ [19], $OsSi_2$ [19] and $IrSi_3$ [19].

The growth kinetics for Reaction 12b (Mn + 1.73 Si → $Mn_{1.73}$) is unknown at this time. Because of the relatively high ΔG° value ($-$ 69.3 kJ mol^{-1}), it is expected that this reaction will occur through a layered growth process. Further investigation needs to be done. Direct formation of $MnSi_{1.73}$ from Mn and Si would be desirable, as well as epitaxial growth of $MnSi_{1.73}$ on Si.

3.2. Determination of band gap value

The optical constants of $MnSi_{1.73}$, i.e. $k(E)$ and $n(E)$, in the photon energy range of $E > 0.7$ eV have been evaluated using the iterative procedure described above. The optical constants corresponding to the energy range $E < 0.7$ eV cannot be evaluated by this method, because Brett's model is valid only for absorbing films (i.e. k for the film is large), whereas, from Fig. 6, the $MnSi_{1.73}$ film is transparent in this photon energy range.

The calculated results of k and n are shown in Fig. 7a and b, respectively. From the values of $k(E)$,

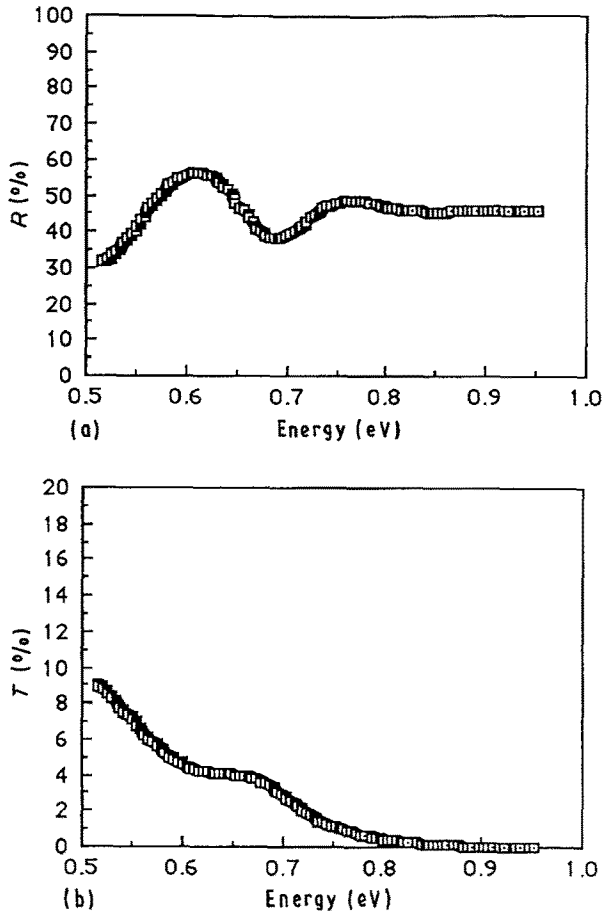

Figure 6 (a) Plot of reflectance R versus photon energy E. (b) Plot of transmittance T versus E. Both transmittance and reflectance were measured from a sample with a 550 nm $MnSi_{1.73}$ film on Si substrate (400 μm).

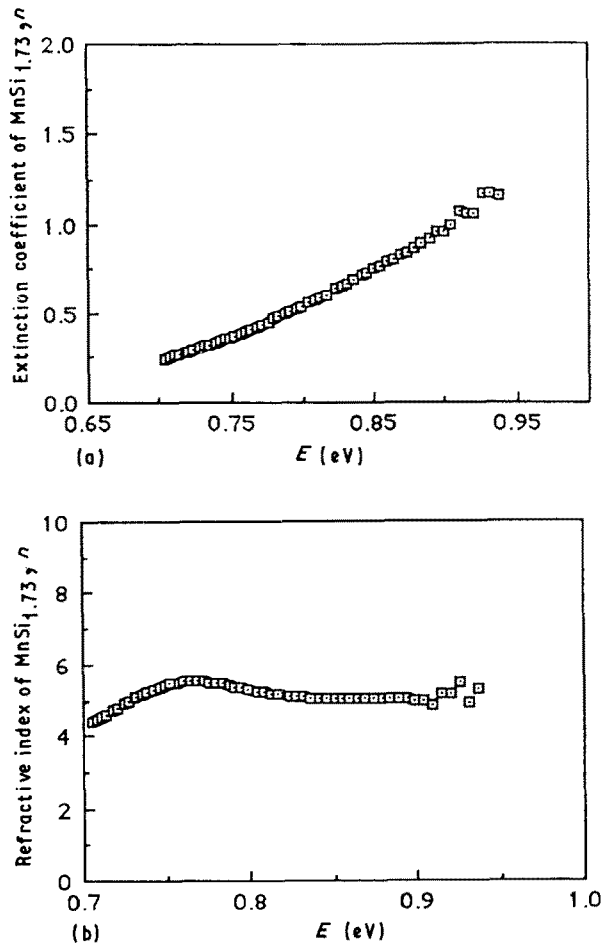

Figure 7 (a) Plot of extinction coefficient k of $MnSi_{1.73}$ versus photon energy E. (b) Plot of refractive index n of $MnSi_{1.73}$ versus E.

the absorption coefficient of $MnSi_{1.73}$, α, was calculated using Equation 2. A plot of α^2 versus photon energy ($E = hc/\lambda$) is shown in Fig. 8. In this figure, an extrapolated straight line was obtained by curve-fitting the data represented by the closed squares. It can be seen that the data do not follow a straight-line

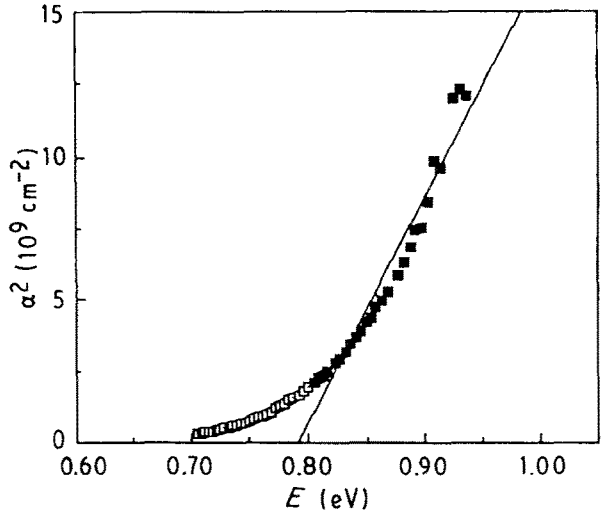

Figure 8 Plot of α^2 versus E for determination of band gap value of $MnSi_{1.73}$: (■) data points used for curve-fitting. The extrapolated intercept of the resulting straight line is between 0.78 and 0.83 eV.

relationship exactly so that the intercepts of the extrapolated line with the energy axis may be in a range, instead of one point. Therefore, the value of band gap determined from this figure is between 0.78 and 0.83 eV. These values are higher than those reported by Bost and Mahan [1], but still in the range of the values calculated by other researchers (0.4–0.9 eV) [5, 6, 8, 24].

It has been found, by direct observation of cross-section TEM specimens, that the thickness of the silicide layer is not uniform due to the polycrystalline nature of the specimen. Surface-energy considerations lead to thermal grooving and surface roughness, where grain boundaries meet an interface or free surface (Fig. 9). The change in thickness, and therefore the non-planar nature of the $MnSi_{1.73}$–Si interface, will affect optical measurements and this may account for the poor curve fit in Fig. 8.

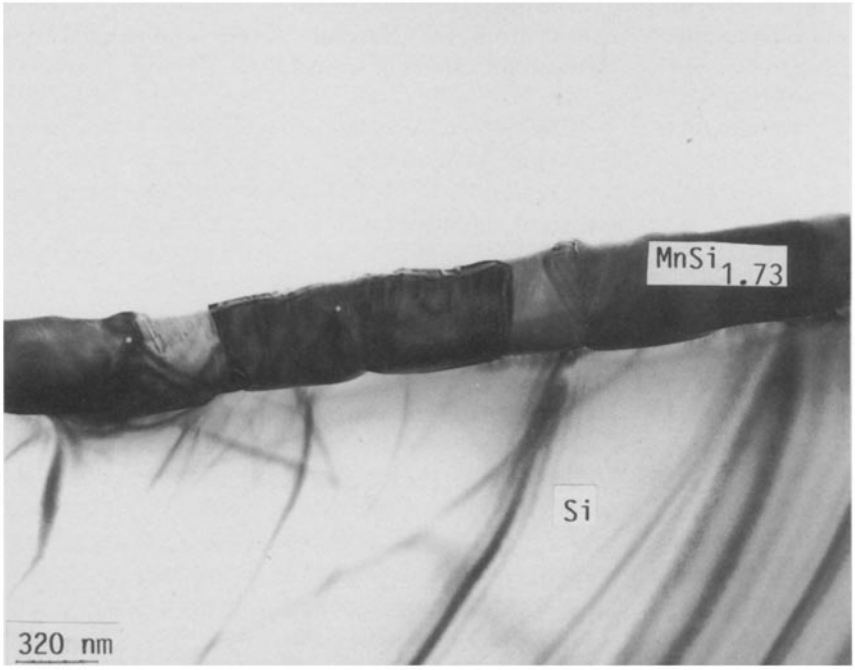

Figure 9 Bright-field TEM micrograph of cross-section specimen of $MnSi_{1.73}$ on Si showing surface roughness at both the $MnSi_{1.73}$–Si interface and the surface.

4. Conclusions

1. $MnSi_{1.73}$ forms in Mn–Si thin-film diffusion couples from MnSi by means of the reaction

$$MnSi + 0.73Si \rightarrow MnSi_{1.73}$$

2. $MnSi_{1.73}$ grows in three dimensions by an island growth mechanism.

3. The structure of $MnSi_{1.73}$ matches best with Mn_4Si_7, with $a = 0.5525$ nm and $c = 1.7465$ nm.

4. The band gap energy of $MnSi_{1.73}$ is between 0.78 and 0.83 eV.

Appendix A: Modification of Brett's model

In Brett's model [13], i.e. an absorbing film on a transparent substrate, the expressions for T and R are

$$T = \exp(-\alpha d)(1 - r_0)(1 - r_1)(1 - r_2) \quad \text{(A1)}$$

$$R = r_0 + \exp(-2\alpha d)[(1 - r_0)^2 r_1 + (1 - r_0)^2(1 - r_1)^2 r_2] \quad \text{(A2)}$$

where α, d, r_0, r_1 and r_2 correspond to α, d, r_0, r and r_s in the modified equations which were used in this study. Since the Si substrate is not completely transparent due to its relatively large thickness, the absorption of Si has been considered by introducing a factor of $\exp(-2\alpha_s d_s)$:

$$T = \exp(-\alpha d)\exp(-\alpha_s d_s)(1 - r_0)(1 - r)(1 - r_s) \quad \text{(A3)}$$

$$R = r_0 + \exp(-2\alpha d)[(1 - r_0)^2 r + (1 - r_0)^2(1 - r)^2 r_s \exp(-\alpha_s d_s)] \quad \text{(A4)}$$

where α and α_s are the absorption coefficients of $MnSi_{1.73}$ and Si, separately; d and d_s are the thickness of the $MnSi_{1.73}$ film and Si substrate, respectively; and r_0, r and r_s represent the reflectivities of each interface shown in Fig. 1.

Appendix B: Derivation of Equations 7–9

The energy flowing, total transmission and reflection in a system allowing multiple internal reflections are schematically shown in Fig. B1 [25]. If the Si specimen has a reflectivity r_s, an absorption coefficient α_s, and a thickness d_s, the total transmission, T, can be expressed by the following equation [29]:

$$T = \frac{(1 - r_s)^2 \exp(-\alpha_s d_s)}{1 - r_s^2 \exp(-2\alpha_s d_s)} \quad \text{(B1)}$$

The total reflection, R, is a sum of all multiple reflections and can be obtained from Fig. B1 as follows:

$$R = r_s + \frac{(1 - r_s)^2 r_s \exp(-2\alpha_s d_s)}{1 - r_s^2 \exp(-2\alpha_s d_s)} \quad \text{(B2)}$$

By combining Equations B1 and B2, r_s can be solved and expressed as

$$r_s = \frac{-(R^2 - 2R - 1 - T^2) + [(R^2 - 2R - 1 - T^2)^2 - 4(2 - R)R]^{1/2}}{2(2 - R)} \quad \text{(B3)}$$

k_s can also be solved by combining Equations B1, B2 and the formula $\alpha = 4\pi k/\lambda$:

$$k_s = -\frac{1}{2}\left[\log\left(\frac{R - r_s}{Rr_s^2 + r_s - 2r_s^2}\right)\right]\left(\frac{\lambda}{4\pi d_s}\right) \quad \text{(B4)}$$

The refractive index for Si (n_s) can also be solved using $r_s = (1 + n_s)^2/(1 - n_s)^2$ since k_s is negligible in this equation:

$$n_s = \frac{1 + r_s^{1/2}}{1 - r_s^{1/2}} \quad \text{(B5)}$$

Acknowledgements

The authors wish to thank Dr M. Brett for valuable discussions with regard to the interpretation of the optical measurements. The assistance of Mr G. McKinnon, Mr K. Westra and Mr A. Mitchell of the Alberta Microelectronic Centre and Mr B. Arnold of the Electrical Engineering Department in preparing and characterizing the thin-film structures is gratefully acknowledged. This research was supported by a grant from the Natural Science and Engineering Research Council of Canada.

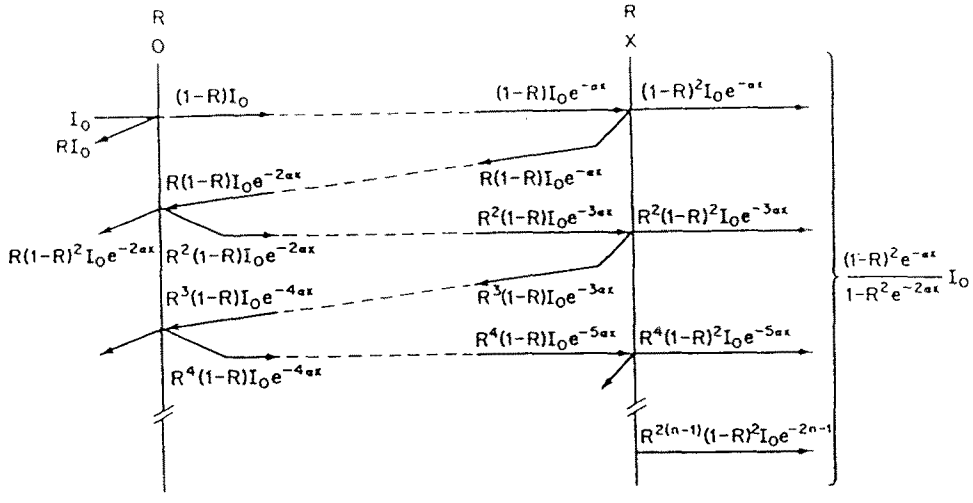

Figure B1 Accounting of energy flow when multiple reflection takes place in an Si wafer [25].

References

1. M. C. BOST and J. E. MAHAN, *J. Electr. Mater.* **16** (1987) 389.
2. *Idem, J. Appl. Phys.* **58** (1985) 2696.
3. *Idem*, unpublished data (1987).
4. R. G. LONG, M. C. BOST and J. E. MAHAN, unpublished data (1988).
5. I. NISHIDA, *J. Mater. Sci.* **7** (1972) 435.
6. I. KAWASUNI, M. SAKATA, I. NISHIDA and K. MASUMOTO, *ibid.* **16** (1981) 355.
7. G. V. SAMSONOV, in "Plenum Press Handbooks of High-Temperature Materials, No. 2: Properties Index" (Plenum, New York, 1964) p. 161.
8. Ch. KRONTIRAS, K. POMONI and M. ROILOS, *J. Phys. D: Appl. Phys.* **21** (1988) 509.
9. M. C. BOST and J. E. MAHAN, *J. Electr. Mater.* **16** (1987) 389.
10. LIN ZHANG and D. G. IVEY, *J. Mater. Res.* in press.
11. D. G. IVEY and G. R. PIERCY, *J. Electron Microsc. Tech.* **8** (1988) 233.
12. J. C. BRAVMAN and R. SINCLAIR, *ibid.* **1** (1984) 53.
13. M. J. BRETT, PhD thesis, University of British Columbia (1985) p. 117.
14. J. D. M. DONNAY and H. M. ONDIK, in "Crystal Data–Determinative Table", Vol. 2 (US Department of Commerce, National Bureau of Standards and the Joint Committee on Powder Diffraction Standards, Washington, D.C., 1973) p. PT-171.
15. O. SCHWOMMA, A. PREISINGER, H. NOWOTNY and A. WITTMAN, *Mh. Chem.* **95** (1964) 1527.
16. H. W. KNOTT, M. H. MUELLER and L. HEATON, *Acta Crystallogr.* **23** (1967) 549.
17. P. VILLARS and L. D. CALVERT, in "Pearson's Handbook of Crystallographic Data for Intermetallic Phases", Vol. 1 (American Society for Metals, Metal Park, 1985) p. 471.
18. H. Q. YE and S. AMELINCKX, in "Modulated Structure Materials", edited by T. Tsakalakos (Nijhoff, Boston, 1984) p. 173.
19. F. M. d'HEURLE and P. GAS, *J. Mater. Res.* **1** (1986) 205.
20. G. V. SAMSONOV and I. M. VINITSKII, in "Handbook of Refractory Compounds" (IFI/Plenum, 1980).
21 T. G. CHART, *High Temp.–High Press.* **5** (1973) 241.
22. M. EIZENBERG and K. N. TU, *J. Appl. Phys.* **53** (1982) 6885.
23. C. S. PETERSON, R. ANDERSON, J. E. BAGLIN, J. DEMPSEY, W. HAMMER, F. M. d'HEURLE and S. J. LAPLACA, *ibid.* **51** (1980) 373.
24. K. E. SUNDSTROM, S. PETERSSON and P. A. TOVE, *Phys. Status Solidi (a)* **20** (1973) 653.
25. J. I. PANKOVE, "Optical Processes in Semiconductors" (Prentice Hall, Englewood Cliffs, 1971) Ch. 4.

Received 27 November
and accepted 10 December 1990